CrossMark

Effect of mechanical mixing method of preparation of polyaniline-transition metal oxide composites on DC conductivity and humidity sensing response

R. Megha[1] · Y. T. Ravikiran[1] · B. Chethan[2] · H. G. Raj Prakash[2] · S. C. Vijaya Kumari[3] · S. Thomas[4]

© Springer Science+Business Media, LLC, part of Springer Nature 2018

Abstract

In the present work, optimized polyaniline-titanium dioxide (PANI-TiO$_2$) and polyaniline-yttrium oxide (PANI-Y$_2$O$_3$) composites were prepared by mechanical mixing of chemically synthesized PANI with TiO$_2$ and Y$_2$O$_3$ transition metal oxides respectively. The Fourier transform infrared spectroscopy (FTIR) analysis confirmed relative decrease in depth of delocalization band of PANI in the composites as compared to that in PANI. The X-ray diffraction (XRD) studies confirmed decrease in degree of crystallinity and increase in inter-chain separation of PANI in the composites as compared to those of PANI. The scanning electron microscopy (SEM) images confirmed relatively more agglomerated and porous granular morphology of the composites as compared to that of PANI. Decrease in DC conductivity of the composites as compared to that of PANI confirmed experimentally and then supported theoretically by one dimensional variable ranging hopping (VRH) model. The PANI-TiO$_2$ and PANI-Y$_2$O$_3$ composites, when studied for their humidity sensing performance, recorded remarkable maximum sensing response of 94 and 96% respectively at 97% RH as compared to 40% of PANI. The response and the recovery time of PANI-TiO$_2$ composite were 95 and 122 s respectively and those of PANI-Y$_2$O$_3$ composite were 50 and 80 s respectively. Humidity sensing stability of the composites tested for a period of 1 month and confirmed.

1 Introduction

Conducting polymers have fascinating potential for technological applications mainly because of their ability to combine both the chemical and the mechanical properties of polymers with the electronic properties of metals and semiconductors [1, 2]. Nowadays, researchers are involved in tuning the electrical properties of such polymers simultaneously trying to overcome their drawbacks such as poor chemical stability and poor mechanical strength by incorporating them with metals or metal oxides via chemical or electrochemical routes [3–5]. Such systems, called organic–inorganic composites or hybrids, have proved to be highly flexible materials in terms of enhancing electrical and mechanical properties due to synergetic effects and thus have offered exciting opportunities for applications in solar cells, super capacitors, sensors and photocatalysis [1, 6]. In the present work, to enhance the scope of such hybrids, PANI, a well-known conducting polymer is preferred as an organic component because of its controllable electrical and chemical properties, simple preparation and low cost [7]. It is a p-type semiconducting material having pseudo orthorhombic/orthorhombic phase and has wide applications in sensors, catalysis, fuel cells, rechargeable batteries, anti-corrosion coating, solar cells, light emitting diodes, super capacitors etc [8, 9]. Among the inorganic components, transition metal oxides are preferred because of their favorable electronic, chemical and mechanical properties and because of which they have found applications in catalysis, fuel cells and electronic devices [10, 11]. Among such transition metal oxides, the two transition metal oxides considered are: (1) Y$_2$O$_3$ of cubic phase, a p-type semiconductor with a wide band gap (5–6 eV) having excellent electrical, thermal, optical,

✉ Y. T. Ravikiran
ytrcta@gmail.com

1 Department of PG Studies and Research in Physics, Government Science College, Chitradurga, Karnataka 577 501, India

2 Department of Physics, JNN College of Engineering, Shivamogga, Karnataka 577 204, India

3 Department of Physics, SJM College of Arts, Science and Commerce, Chitradurga, Karnataka 577 501, India

4 International and Inter University Centre for Nanoscience and Nanotechnology, Mahatma Gandhi University, Kottayam, Kerala 686 560, India

chemical and mechanical properties and is widely used in red-light-emitting phosphors, yttrium–aluminum garnets (YAG), lithium batteries and yttria stabilized zirconia (YSZ) thin films [12–14]. (2) The rutile TiO_2 of tetragonal phase, an n-type semiconductor with a wide band gap (3–4 eV) and large dielectric constant (~ 114) having excellent photocatalytic and electric properties and hence has found applications in catalysis, Fuel cells, dielectric ceramics, solar cells and optoelectronic devices [15, 16]. Because of all these favorable properties of PANI, TiO_2 and Y_2O_3, we prepared the PANI-TiO_2 and PANI-Y_2O_3 hybrid composites by mechanical mixing of chemically synthesized PANI with the respective metal oxides. Some such PANI based metal oxide composites synthesized by in-situ polymerization method have been reported recently [17–20]. In those cases where the method of preparation was the in-situ polymerization, achieving synergy was met with some inherent drawbacks: in some cases, the macromolecular chains of the polymer may get attached to the filler which may not allow the filler to form an interconnecting network thus counteracting the intended synergistic effects [21], and the method, the nature of which is such, cannot be applied for bulk production of the composites. So, if an alternate, simpler, suitable and cost effective method of synthesis like mechanical mixing is used, that method, besides overcoming those drawbacks would enable better formation of hybrid structures in the form of composites and interfaces which would in turn help in tailoring flexible composites for industrial production having advantageous electrical, chemical, and mechanical properties [22] and hence their applications in sensors and lithium ion batteries can be widened [23, 24].

So in the present work, a first of its kind, synergistic effects on DC conductivity and resistive type room temperature humidity sensing behavior of PANI-TiO_2 and PANI-Y_2O_3 composites prepared by mechanical mixing are studied. For the purpose, chemically synthesized PANI and 10 wt% of the respective transition metal oxide were mechanically mixed to prepare PANI-TiO_2 and PANI-Y_2O_3 composites and then structurally and morphologically characterized. Then, DC conductivity of PANI and the composites were experimentally measured and correlated with structural studies. Further, the experimental results were comparatively studied theoretically through the parameters of one dimensional VRH model so as to get a clear insight into the charge transport mechanism [25, 26]. As a typical application, we have comparatively studied room temperature humidity sensing performance of PANI and the composites as that would be helpful for purpose oriented device fabrication on an industrial scale.

2 Materials and methods

2.1 Materials

Aniline ($C_6H_5NH_2$), Ammonium persulfate (($NH_4)_2S_2O_8$), Ferric chloride ($FeCl_3$), Hydrochloric acid (HCl), Acetone (C_3H_6O), Yttrium oxide (Y_2O_3), Titanium dioxide (TiO_2), all of analytical grade reagents were purchased from s.d. Fine Chemicals, Mumbai, India. Aniline monomer was doubly distilled before use.

2.2 Preparation of PANI and the composites

To synthesize pristine PANI, a mixture of 20 mL of 35 wt% of HCl and 2.0 g of aniline was dispersed in 200 mL of distilled water with [HCl]/[aniline] ratio at 6. Then, 4.8 g of ammonium persulfate (($NH_4)_2S_2O_8$) followed by 3.75 g of ferric chloride ($FeCl_3$) was added drop wise into the solution with continuous stirring for 3 h and then allowed to polymerize at room temperature for at least 8–10 h. The reaction product was collected by centrifugation and washed successively with 1M HCl, deionized water and acetone until the filtrate became colorless and then dried in vacuum at 60 °C for 24 h till a dark green powder of PANI was obtained.

The prepared PANI and 10 wt% Y_2O_3 were mixed mechanically in a vibration mill (Make: Techno-search Instruments, Mumbai, India) for 10–15 min to get a homogeneous mixture of PANI-Y_2O_3 composite. The PANI-TiO_2 composite was similarly prepared.

2.3 Characterization

The FTIR spectra of pristine PANI and the composites were recorded using Nicolet 750 FT-IR spectrometer in KBr medium at room temperature for which each sample in powder form was mixed with KBr in the ratio of 1:25 by weight and was ground to ensure uniform dispersion. Then, the mixed powders of the samples were pressed separately in a cylindrical dye to obtain discs of approximately 1 mm thickness. The XRD pattern of each sample was obtained by employing Siemens D-5000 powder X-ray diffractometer with CuKα source radiation ($\lambda = 1.54 \times 10^{-10}$ m). The diffractograms were recorded in terms of 2θ in the range of 10–80° with a scanning rate of 2°/min. For SEM studies, each powder sample was dispersed on the surface of carbon tape mounted on aluminium tab and conducting gold was sputtered on the sample to avoid charging at the sample surfaces, and hence, selected areas were photographed using Hitachi S-520 scanning electron microscope.

2.4 DC conductivity measurements

To study the DC conductivity of PANI and the composites, each sample in powder form was pressed under hydraulic pressure of about 4 tons to get cylindrical pellets (8 mm dia × 1 mm thick, with silver electrodes). Then, variation of resistance with temperature of each sample was measured using an interfaced programmable digital multimeter (Hioki DT 4252, Japan).

2.5 Humidity sensing measurements

For humidity sensing measurements of pellet of each sample, specially designed glass chambers, each of which was maintained at a specific relative humidity and monitored using humidity meter (Mextech-DT-615) were used and are shown Fig. 1. Each chamber was fitted at the top with a cork through which the electrodes connected to the pellet pass through. The other ends of the electrodes were connected to an interfaced programmable digital multimeter (Hioki DT 4252, Japan) to record resistance changes before and after exposing the sample to humidity in each jar.

3 Results and discussion

3.1 Fourier transform infrared spectroscopy

The FTIR spectra of PANI, TiO_2, Y_2O_3, PANI-TiO_2 and PANI-Y_2O_3 composites are shown in Fig. 2. The FTIR spectrum of pristine PANI with all its characteristic absorption bands is shown in Fig. 2a. The appearance of broad band at 3438 cm^{-1} attributed to the N–H stretching vibration, the band at 1495 cm^{-1} attributed to C=C stretching vibration of benzenoid ring and the relatively less intense absorption band at 1570 cm^{-1} attributed to C=C stretching vibration of quinoid ring, all confirm the emeraldine salt form of PANI [27, 28]. Also, the other bands of PANI at 3227, 1295, 1141, 820 and 727 cm^{-1} are attributed respectively to the C–H stretching vibration, C–N stretching of imine and secondary amine, C–H in-plane bending vibration, 1,4-coupling of aromatic ring and C–H out-plane bending vibration [29]. The characteristic absorption bands of TiO_2 (Fig. 2b) at 647 and 418 cm^{-1} are attributed to Ti-O stretching vibration [6]. The characteristic absorption band of Y_2O_3 (Fig. 2d) at 562 cm^{-1} is attributed to Y–O stretching vibration [12].

The FTIR spectrum of PANI-TiO_2 composite (Fig. 2c) shows slightly shifted characteristic bands of PANI mentioned above as well as those of TiO_2 while the FTIR spectrum of PANI-Y_2O_3 (Fig. 2e) composite shows presence of slightly shifted characteristic bands of PANI and that of Y_2O_3 confirming interfacial interaction of each of the transition metal oxide with PANI in the respective composite [30]. This interaction may be due to the hydrogen bonding of oxygen atoms on the surface of transition metal oxides with NH of PANI which makes oxide particles be embedded in PANI chains [31] and this mechanism of interaction is illustrated in Fig. 3.

An important revelation from the comparative study of FTIR spectra is that the depth of the band at 3438 cm^{-1}
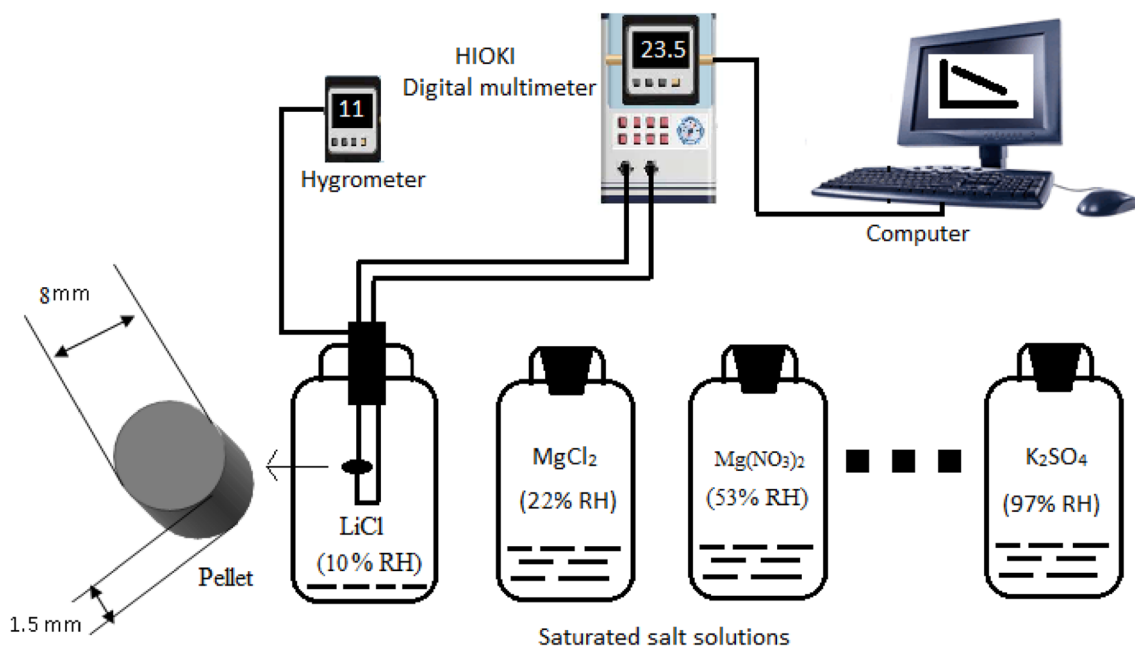

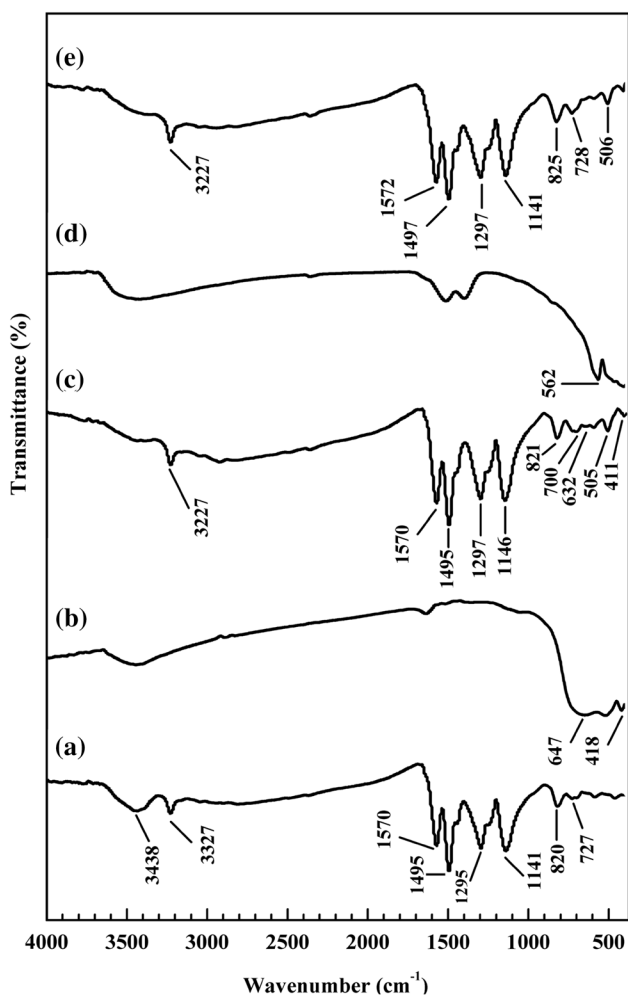**Fig. 1** Schematic diagram of experimental setup for humidity sensing studies

Fig. 2 FTIR spectra of (*a*) pristine PANI (*b*) TiO$_2$ (*c*) PANI-TiO$_2$ composite (*d*) Y$_2$O$_3$ and (*e*) PANI-Y$_2$O$_3$ composite
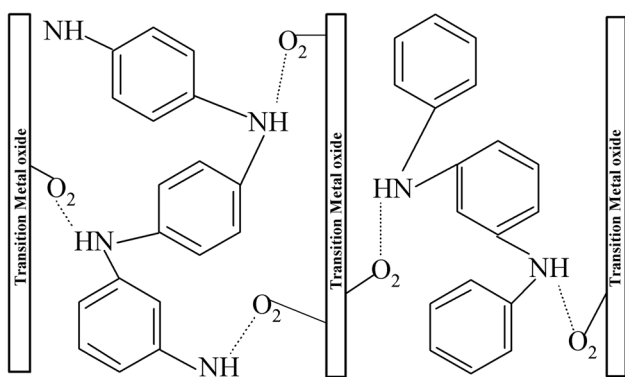

Fig. 3 An illustration of mechanism of interaction

attributed to N–H stretching vibration of PANI in the composites has almost disappeared confirming strong interaction between PANI and metal oxides in the respective composites. So, consequent significant implication is that electron

density of PANI chains in the composites has decreased resulting in decrease in their conductivity [4]. Also, a lesser depth in charge delocalization band of PANI at 1141 cm^{-1} in the composites as compared to that of pure PANI indicates weakened π-electron delocalization and consequent decrease in conductivity of the composites [29, 32].

3.2 X-ray diffraction

The XRD patterns of pristine PANI, TiO$_2$, Y$_2$O$_3$, PANI-TiO$_2$ and PANI-Y$_2$O$_3$ composites are shown in Fig. 4. The XRD pattern of PANI (Fig. 4a) shows its characteristic amorphous peak at $2\theta = 19°$ and semi crystalline peak at $2\theta = 25.8°$ assigned respectively to (100) and (110) planes which are attributed to the periodicity parallel and perpendicular to the polymer chains. All these characteristic features confirm semicrystalline pseudo-orthorhombic emaralidine salt form of PANI and are in conformity with those published in earlier literatures [3, 33]. The XRD pattern of rutile TiO$_2$ (Fig. 4b) shows its characteristic peaks at
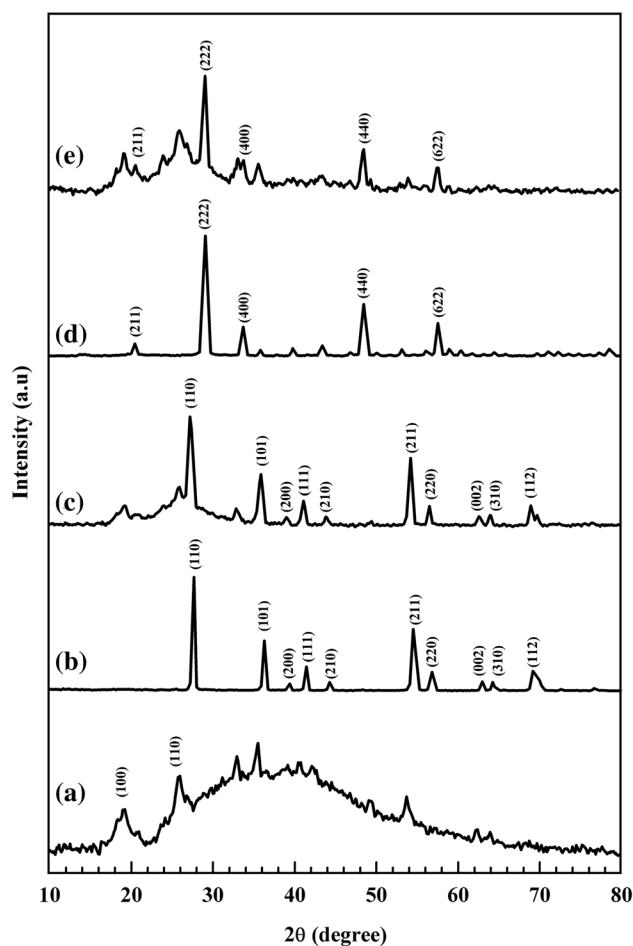

Fig. 4 XRD patterns of (*a*) pristine PANI (*b*) TiO$_2$ (*c*) PANI-TiO$_2$ composite (*d*) Y$_2$O$_3$ and (*e*) PANI-Y$_2$O$_3$ composite

$2\theta = 27.6°$, $36.3°$, $39.4°$, $41.4°$, $44.2°$, $54.6°$, $56.8°$, $62.9°$, $64.2°$, and $69.1°$ assigned respectively to the planes (110), (101), (200), (111), (210), (211), (220), (002), (310) and (112) as confirmed from JCPDS file NO 21-1276. The XRD pattern of cubic phase Y_2O_3 (Fig. 4d) shows its characteristic peaks at $2\theta = 20.4°$, $28.9°$, $33.5°$, $48.4°$, and $57.62°$ assigned respectively to the planes (211), (222), (400), (440) and (622) as confirmed from JCPDS file NO 41-1105. All these characteristic peaks of TiO_2 and Y_2O_3 have also been confirmed from earlier literatures [12, 15].

The XRD patterns PANI-TiO_2 and PANI-Y_2O_3 composites (Fig. 4c, e) show the characteristic peaks of both PANI and the respective metal oxide with no additional peaks or disappearance of peaks suggesting that Y_2O_3 and TiO_2 have retained their individual structures in the respective composite and are in interfacial interaction with PANI in the respective composite. These facts have also been supported by earlier literatures [34, 35].

The XRD parameters namely, the d-spacing (d), the inter-chain separation (R) and percentage of degree of crystallinity (χ_c) for pristine PANI and for PANI in the composites have been calculated using the following formulae:

Average crystallite size of the composites was determined by Scherrer's formula given by Eq. (1) [2]

$$L = \frac{K\lambda}{\beta \cos\theta} \tag{1}$$

where K is the shape factor, which is equal to 0.9, β is the full width at half maxima (FWHM) in radian and λ is the X-ray wavelength.

The inter-chain separation length (R) of PANI and the composites can be estimated from the relation given by Klug and Alexander [36] as given in Eq. (2)

$$R = \frac{5}{8}\left[\frac{\lambda}{\sin\theta}\right] \tag{2}$$

The percentage of degree of crystallinity (χ_c) has been calculated from the Eq. (3) [37]

$$\chi_c\% = \frac{(I_{cr} - I_{am})}{I_{cr}} \times 100\% \tag{3}$$

where I_{cr} is the intensity of the crystalline peak and I_{am} is the intensity of the amorphous peak. The parameters calculated from above equations are given in Table 1. A comparative study of the parameters infers that the d-spacing and the inter-chain separation of PANI in the composites have increased while the percentage of degree of crystallinity has decreased as compared to those of PANI suggesting decrease in conductivity of the composites [36]. The average crystallite size of each composite was found to be 15 nm.

Table 1 Values of d-spacing (d), inter-chain separation (R) and degree of crystallinity (χ_c) of pristine PANI and of PANI in the composites

Samples	d (Å)	R (Å)	χ_c (%)
Pristine PANI	4.64	5.80	42
PANI-TiO_2	4.65	5.81	40
PANI-Y_2O_3	4.66	5.82	34

3.3 Scanning electron microscopy

The SEM images of PANI, TiO_2, Y_2O_3, PANI-TiO_2 and PANI-Y_2O_3 composites are shown in Fig. 5. The SEM image of pristine PANI (Fig. 5a) shows clusters of globular grains. The SEM image of TiO_2 (Fig. 5b) shows irregular spherical structure with good homogeneity while SEM image of Y_2O_3 (Fig. 5c) shows small flake like granular structure. The SEM image of each composite (Fig. 5d, e) compared to that of PANI shows increased agglomeration, good homogeneity and porous granular morphology in which the transition metal oxide particles are embedded in PANI matrix [38, 39]. The average grain size of the PANI and the composites were determined using image J software. The accuracy of average grain size so obtained in each case was verified by fitting the average grain size of each of PANI and the composites to normal distribution function. The grain size so obtained for PANI was 1.6 μm while that for each composite was 0.8 μm. This remarkable reduction in grain size of each composite to half that of pure PANI, acquired just by mechanical mixing method is noteworthy because that has resulted in increase in grain boundaries and pores in their structure thus offering more active sites for water absorption [40].

3.4 DC conductivity analysis

For the comparative analysis of DC conductivity of PANI and the composites, the DC conductivities were calculated using Eq. (4)

$$\sigma_{dc} = \left(\frac{d}{RA}\right) \tag{4}$$

where d, A and R are the respective thickness, area and resistance of the samples. Then the plot of variation of DC conductivity with temperature for each sample was obtained (Fig. 6) which shows that the conductivity of all the samples has increased with increase in temperature confirming their semiconducting behavior [31]. Further, the measured temperature dependent conductivity was fitted to Arrhenius Eq. (5) and then activation energies were calculated from the slope of the plots.

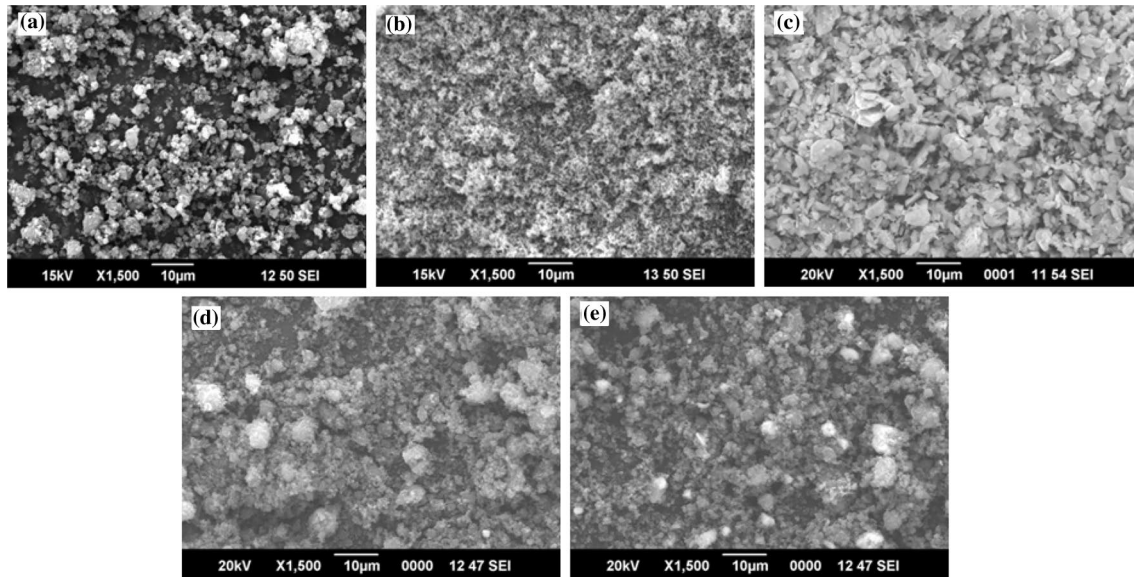$$\sigma(T) = \sigma_0 \exp\left(\frac{-E_a}{2kT}\right) \tag{5}$$

Fig. 5 SEM images of **a** pristine PANI, **b** TiO$_2$, **c** Y$_2$O$_3$, **d** PANI-TiO$_2$ composite and **e** PANI-Y$_2$O$_3$ composite
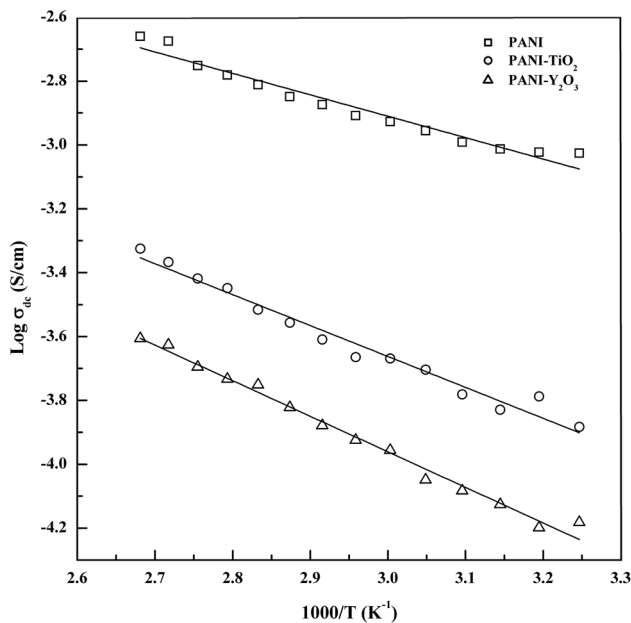

Fig. 6 Temperature dependence of DC conductivity of PANI and the composites. The solid lines are the fits obtained using Arrhenius equation

where σ_0 is the pre-exponential factor, E_a is the activation energy and k is the Boltzmann constant. The activation energy for PANI, PANI-TiO$_2$ and PANI-Y$_2$O$_3$ are 0.13, 0.19 and 0.21 eV respectively. So, the activation energy of the composites has increased as compared to that of PANI which implies decrease in their conductivity [38]. The decreased conductivity of the composites may be understood as follows: As more and more number of N atoms of PANI chains

in the composite get involved in bond formation with oxygen atoms of respective transition metal oxide, growth of PANI chains in the composite might be restricted, thus obstructing the hopping of charge carriers resulting in decrease in hopping length and consequent decrease in conductivity [2, 19]. The observed DC conducting behavior can be clearly understood theoretically in-terms of variation of charge transport parameters obtained by fitting the experimentally measured DC conductivity data of PANI and the composites to one dimensional variable range hopping (VRH) model. For the purpose, the Ziller Eqs. (6), (7) (8) and (9) were made use of [25, 26, 41]

$$\sigma(T) = \sigma_0 \exp\left(\frac{-T_0}{T}\right)^{1/2} \tag{6}$$

where T_0 is the respective characteristic temperature of PANI and the composites which was obtained as the slope of the respective linear plot of log σ versus $T^{-1/2}$ (Fig. 7).

The localization length (α^{-1}) was calculated using Eq. (7)

$$T_0 = \frac{8\alpha}{N(E_F)Zk} \tag{7}$$

where Z is the number of nearest neighboring chains (~4), k is Boltzmann constant and $N(E_F)$ is the density of states per electron volt (2-ring unit suggested for polyaniline) [25, 26].

The probable hopping distance (R) and charge hopping energy (w) were calculated using the Eqs. (8) and (9),

$$R = \left(\frac{T_0}{T}\right)^{1/2}\left(\frac{\alpha^{-1}}{4}\right) \tag{8}$$
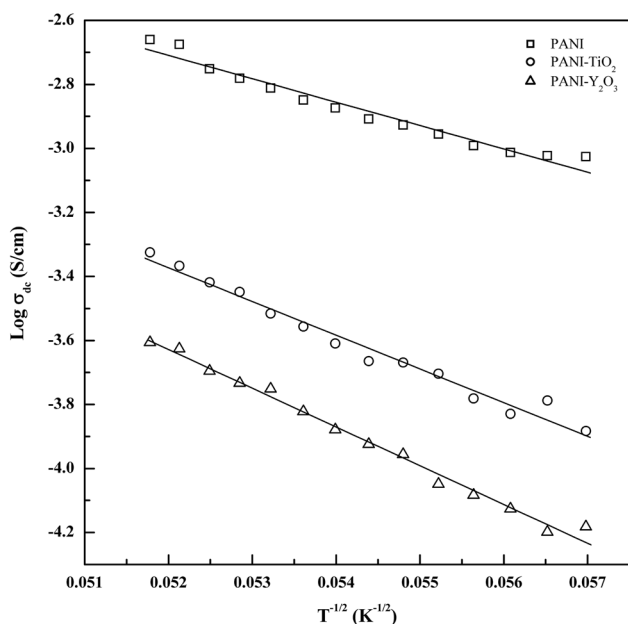
Fig. 7 Temperature dependence of DC conductivity of PANI and the composites. The solid lines are the fits obtained using Ziller equation

$$w = Zk\left(\frac{T_0}{16}\right) \tag{9}$$

The numerical values of transport parameters so calculated for PANI and the composites are given in Table 2. As is clear from the Table, charge localization length and the most probable hopping distance of each of the composite has decreased where as hopping energy has increased as compared to those of PANI, all of which summarily suggest decreased conductivity of the composites. Thus, the theoretically arrived conclusions agree very well with the experimental results and also correlate very well with the structural characterization studies. So, the DC conducting behavior of the composites prepared by mechanical mixing can also be clearly understood through the parameters of one dimensional VRH model.

3.5 Humidity sensing response

The variation in resistance with relative humidity in the range 10–97% RH for PANI and the composites were measured and the related plots are shown in Fig. 8.

Table 2 Transport parameters of PANI and the composites

Samples	α^{-1} (nm)	R (nm)	w (eV)
Pristine PANI	1.92	3.00	0.26
PANI-TiO$_2$	1.21	2.38	0.41
PANI-Y$_2$O$_3$	0.92	2.09	0.54

The humidity sensing response at room temperature of each of PANI and the composites was calculated using the following equation [7].

$$S_H = \frac{R_0 - R_{RH}}{R_0} \times 100 \tag{10}$$

where R_0 is the resistance of the samples before exposure to moisture (dry air with 10% RH) and R_{RH} is the resistances at various % RH. A sensing response of 40 at 97% RH for PANI was observed which agrees very well with the reported literature [7]. But in striking contrast, the maximum sensing response obtained at the same % RH was 94% for PANI-TiO$_2$ composite and 96% for PANI-Y$_2$O$_3$ composite. So, the composites have shown a remarkable improvement in humidity sensing response compared to that of PANI. This resistive type humidity sensing behavior of the composites may be understood as follows: Under dry conditions, mobility of loosely bound charge carriers in the polymer chains may be restricted due to tendency of the polymer chain to curl into compact form. But as humidity increases, due to open porous structure of the composites as revealed by their SEM images, the polymer chains get uncurled to form straight chains which are aligned with respect to each other resulting in the faster hopping of charge carriers leading to decreased resistance of the composites and hence increase in their sensing response [3]. Mechanism of sensing is illustrated in Fig. 9.
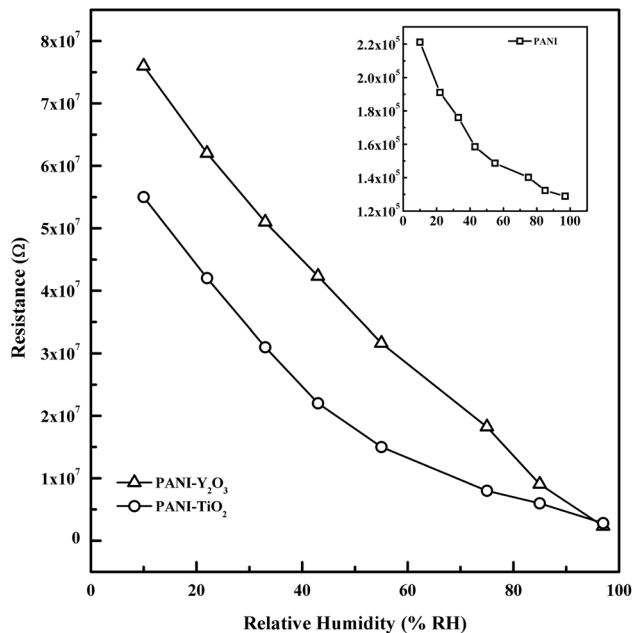

Fig. 8 Variation of resistance with relative humidity for PANI and the composites
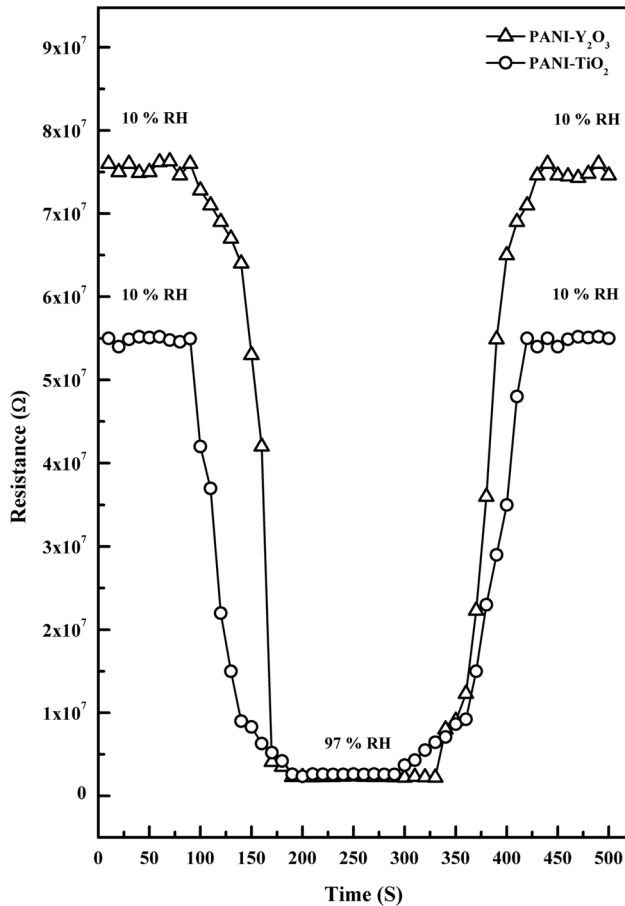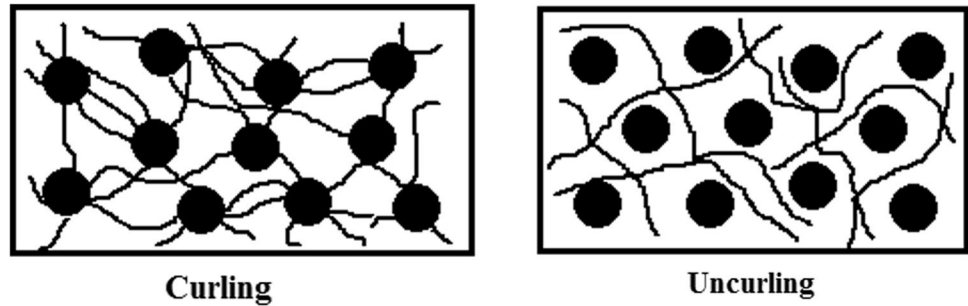
Fig. 9 An illustration of humidity sensing mechanism

Curling   Uncurling

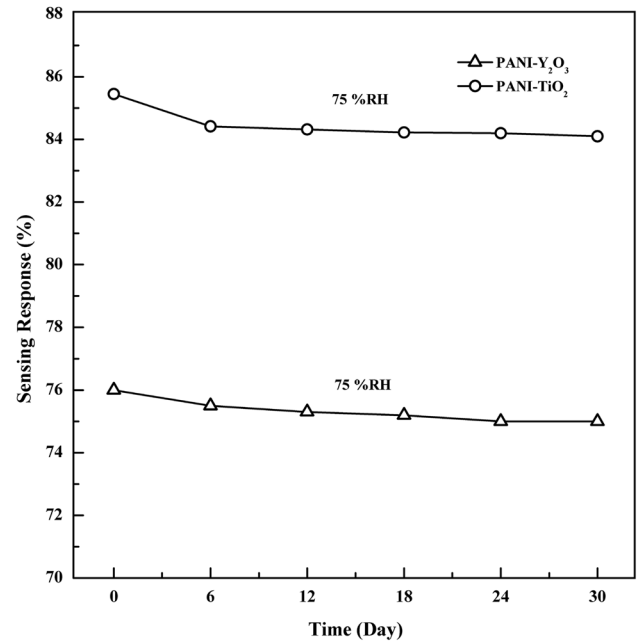**Fig. 10** Response and recovery characteristic curves of the composites

Fig. 11 Stability of the composites

samples were moved from 97% RH to dry air, the switching time being 1 s for determining both response and recovery time. The delay in recovery time is attributed to the heat of adsorption being higher than the heat of desorption because, in case of humidity sensing, adsorption is a spontaneous exothermic process where as desorption is an endothermic process. Desorption is somewhat delayed due to the higher bonding energy between the adsorbed water molecules and the sensing surface [42, 43].

To examine the practical viability of the composites for devising them as sensors, variation of sensing response at 75% RH after every 1 week for 1 month were studied for both the composites separately and the related plots are shown in Fig. 11 which show that each sample (PANI-TiO_2 and PANI-Y_2O_3 composite) had stable sensing ability during that period. So, the two composites under study prepared by mechanical mixing have proved to be efficient and stable humidity sensing materials at room temperature and can be used for device fabrication.

The humidity response and recovery characteristics of PANI-TiO_2 and PANI-Y_2O_3 composites were studied for which two chambers, one with pure dry air (10% RH) and another with 97% RH were maintained separately and the related characteristic curves for both the composites are shown in Fig. 10. A response time of 50 s for PANI-TiO_2 composite and 95 s for PANI-Y_2O_3 composite were recorded when the samples were moved from dry air to 97% RH. A recovery time of 122 s for PANI-TiO_2 composite and 80 s for PANI-Y_2O_3 composite were recorded when the

4 Conclusions

In conclusion, in a study first of its kind, PANI-TiO$_2$ and PANI-Y$_2$O$_3$ hybrid composites prepared by mechanical mixing were comparatively studied for their DC conductivity and humidity sensing response. The PANI-TiO$_2$ and PANI-Y$_2$O$_3$ composites prepared by mechanical mixing have shown remarkable sensing response at room temperature as well as good response and recovery times and stability. The sensors based on these composites have the major advantage over other humidity sensors prepared by in situ polymerization because of the possibility they offer for fabricating efficient, cost effective and stable humidity sensing devices on an industrial scale. Another significance of the work is that the transport properties of the composites prepared by mechanical mixing understood through VRH model can be a guiding example for extending it to understand transport properties of other composites which in turn helps in their selection in multi functional devices.

References

1. R. Megha, Y.T. Ravikiran, S.C. Vijaya Kumari, S. Thomas, Appl. Phys. A Mater. Sci. Process **123**, 245 (2017)
2. R. Megha, S. Kotresh, Y.T. Ravikiran, C.H.V.V. Ramana, S.C. Vijaya Kumari, S. Thomas, Compos. Interfaces **24**, 55 (2017)
3. S. Kotresh, Y.T. Ravikiran, S.C. Vijaya Kumari, H.G. Raj Prakash, S. Thomas, Adv. Mater. Lett. **6**, 641 (2015)
4. B.K. Sharma, N. Khare, S.K. Dhawan, H.C. Gupta, J. Alloys Compd. **477**, 370 (2009)
5. S. Kotresh, Y.T. Ravikiran, S.C. Vijaya Kumari, T. Chandrasekhar, Ch.V.V. Raman, S. Thomas, Mater. Manufact. Process **31**, 1976 (2016)
6. R. Megha, Y.T. Ravikiran, S.C. Vijaya Kumari, T. Chandrasekhar, S. Thomas, Polym. Comp. https://doi.org/10.1002/pc.24375
7. S. Kotresh, Y.T. Ravikiran, H.G. Raj Prakash, C.H.V.V. Ramana, S.C. Vijayakumari, S. Thomas, Cellulose **23**, 3177 (2016)
8. D.S. Dhawale, D.P. Dubal, V.S. Jamadade, R.R. Salunkhe, S.S. Joshi, C.D. Lokhande, Sensors Actuators, B Chem. **145**, 205 (2010)
9. R. Borah, S. Banerjee, A. Kumar, Synth. Met. **197**, 225 (2014)
10. Y. Wakabayashi, J. Phys. Condens. Matter. **23**, 483001 (2011)
11. S. Walia, S. Balendhran, H. Nili, S. Zhuiykov, G. Rosengarten, Q.H. Wang, M. Bhaskaran, S. Sriram, M.S. Strano, K.K. Zadeh, Prog. Mater. Sci. **58**, 1443 (2013)
12. M. Faisal, S. Khasim, Polym. Sci. Ser. A **56**, 366 (2014)
13. G. Korotcenkov, Mater. Sci. Eng. B Solid-State Mater. Adv. Technol. **139**, 1 (2007)
14. M. Aghazadeh, M. Hosseinnifard, M.H. Peyrovi, B. Sabour, J. Rare Earths **31**, 281 (2013)
15. L. Tang, Y. Deng, G. Zeng, W. Hu, J. Wang, Y. Zhou, J. Wang, J. Tang, W. Fang, J. Alloys Compd. **662**, 516 (2016)
16. T. Busani, R.A.B. Devine, Semicond. Sci. Technol. **20**, 870 (2005)
17. S.C. Nagaraju, A.S. Roy, G. Ramgopal, Measurement **60**, 214 (2015)
18. M. Faisal, S. Khasim, E. Conductivity, Dielectric behavior and Emi shielding effectiveness of polyaniline-yttrium oxide composites. Bull. Korean Chem. Soc. **34**, 99–106 (2013)
19. A. Mostafaei, A. Zolriasatein, Prog. Nat. Sci. Mater. Int. **22**, 273 (2012)
20. S.C. Nagaraju, A.S. Roy, A.L. Latha, G. Ramgopal, Ferroelectr. Lett. Sect. **43**, 96 (2016)
21. D.G. Papageorgiou, I.A. Kinloch, R.J. Young, Carbon. **95**, 460 (2015)
22. M. Dhingra, S. Shrivastava, P.S. Kumar, S. Annapoorni, Compos. Part B Eng. **45**, 1515 (2013)
23. J. Huang, T. Yang, Y. Kang, Y. Wang, S. Wang, J. Nat. Gas Chem. **20**, 515 (2011)
24. H. Zheng, N.M. Ncube, K. Raju, N. Mphahlele, M. Mathe, Springerplus. **5**, 630 (2016)
25. B.I. Nandapure, S.B. Kondawar, M.Y. Salunkhe, A.I. Nandapure, Adv. Mater. Lett. **4**, 134 (2013)
26. S.S. Umare, M.M. Huque, M.C. Gupta, S.G. Viswanath, J. Macromol. Sci. Part A. **32**, 281 (2006)
27. M. Khalid, M.A. Tumelero, V.C. Zoldan, C.C. Pla Cid, D.F. Franceschini, R.A. Timm, L.T. Kubota, S.A. Moshkalev, A.A. Pasa, RSC Adv. **4**, 34168 (2014)
28. J.P.B. Ontolan Jr., P.A.M. Alcantara, R.M. Vequizo, M.K. Odarve, B.R.B. Sambo, Phys. Status Solidi. **12**, 580 (2015)
29. N. VijayaKumar, E. Subramanian, D.P. Padiyan, Synth. Met. **162**, 126 (2012)
30. S. Nasirian, H.M. Moghaddam, Polymer **55**, 1866 (2014)
31. M. Khairy, Synth. Met. **189**, 34 (2014)
32. S. Quillard, G. Louarnm, S. Lefrant, A.G. Macdiarmid, Phys. Rev. B Condens. Matter. **50**, 12496 (1994)
33. S. Srivastava, S. Kumar, V.N. Singhh, M. Singh, Y.K. Vijay, Int. J. Hydrogen Energy. **36**, 6343 (2011)
34. R.M. Khafagy, J. Alloys Compd. **509**, 9849 (2011)
35. T. Pandiyarajan, R.V. Mangalaraja, B. Karthikeyan, Spectrochim. Acta Part A Mol. Biomol. Spectrosc. **147**, 280 (2015)
36. S. Bhadra, N.H. Kim, K.Y. Rhee, J.H. Lee, Polym. Int. **58**, 1173 (2009)
37. S. Chapi, S. Raghu, H. Devendrappa, Ionics **22**, 803 (2016)
38. S. Sultana, M.Z. Rafiuddin, K. Khan, Umar, J. Alloys Compd. **535**, 44 (2012)
39. D. Wei, R. Dave, R. Pfeffer, J. Nanopart. Res. **4**, 21 (2002)
40. V. Jeseentharani, L. Reginamary, B. Jeyaraj, A. Dayalan, K.S. Nagaraja, J. Mater. Sci. **47**, 3529 (2012)
41. B. Nandapure, S. Kondawar, M. Salunkhe, A. Nandapure, J. Compos. Mater. **47**, 559 (2012)
42. J.G. Wang, L.X. Zhang, J. Yin, L.X. Zhao, L.J. Bie, Layered K$_{(1.5}$Eu$_{0.5)}$Ta$_3$O$_{10}$ for humidity sensor. Measurement **82**, 151 (2016)
43. V.R. Khadse, S. Thakur, K.R. Patil, P. Patil, Sens. Actuators B Chem. **203**, 10 (2014)